

A Two-Stage Optimization Approach to Safe-by-Design Planning for Autonomous Driving

Francisco Eiras*, Majd Hawasly*, Stefano V. Albrecht*[†], Subramanian Ramamoorthy*[†]

*FiveAI Ltd, UK, {firstname.lastname}@five.ai

[†]School of Informatics, University of Edinburgh, UK

Abstract—Lessons learned from the increasing diversity of road trial deployments of autonomous vehicles have made clear that guaranteeing safety of driving decisions is a crucial bottleneck on the path towards wider adoption. A promising direction is to pose safety requirements as planning constraints in nonlinear optimization problems for motion synthesis. However, many implementations of this approach are limited by uncertain convergence and local optimality of the solutions achieved, affecting overall robustness. In this paper, we propose a novel two-stage optimization framework: in the first stage, we find a global but approximate solution to a Mixed-Integer Linear Programming (MILP) formulation of the motion synthesis problem, the output of which initializes a second Nonlinear Programming (NLP) stage. The MILP stage enforces hard constraints including safety and road rules, while the NLP stage refines that solution within safety bounds to make it feasible with respect to vehicle dynamics and smoothness. We demonstrate the usefulness of our framework through experiments in complex driving situations, showing it outperforms a state of the art baseline in terms of convergence, comfort and progress metrics.

I. INTRODUCTION

With the rapid advancement of Autonomous Vehicle (AV) technology it is becoming increasingly clear that robustly guaranteeing safety across diverse driving scenarios is essential to its wider adoption, with practitioners recognizing the need for ensuring safety *by design* [21, 19]. Performing safe real-time planning in this way, in systems that must robustly achieve tight integration with scene perception and prediction of agent behaviors [2], has continued to be an open challenge for the community. An enticing approach motivated by the ability to collect driving data from millions of miles driven by sensorized vehicles is to exploit machine learning methods, such as in an imitation learning paradigm [6, 7]. However, it has been difficult to provide safety guarantees when policies are learned through such methods, particularly given noisy data and fault-susceptible real time perception. Initial works aimed at providing robustness guarantees of neural networks, while encouraging, remain limited in scope compared to the scale of the models required in practical systems [17, 4].

The multi-dimensional requirements associated with planning in AVs are inherently hierarchical in nature. The core concern of non-collision with other road users and obstacles, in the interest of passenger safety, is a hard constraint. Other secondary concerns, such as continued progress towards a destination, comfort or power management, imply softer constraints. Some planning methods, including many reinforcement learning formulations and some forms of unconstrained trajectory optimization, expect the hierarchy to be resolved implicitly

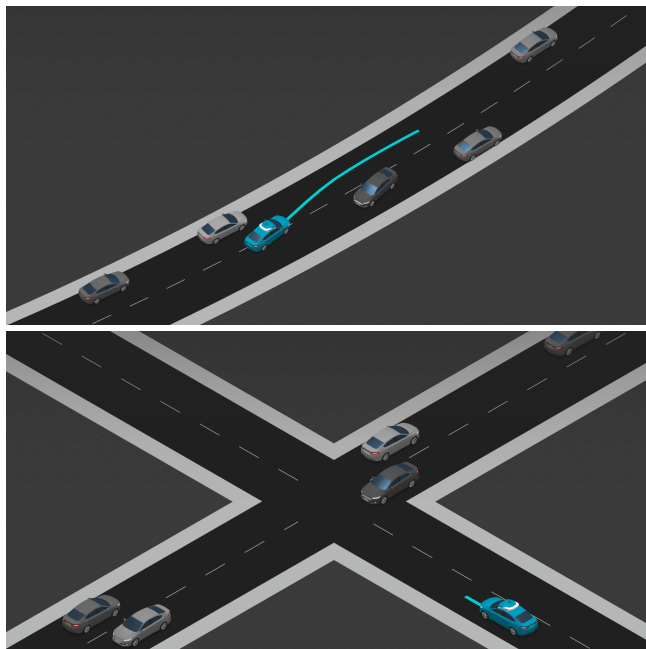


Fig. 1: *Simulated driving situations: Top – overtaking of static vehicles with an oncoming vehicle in residential driving; Bottom – unprotected right turn in a junction*

through the design of the optimization objective [33, 18]. However, such approaches tend to be brittle in enforcing the aforementioned safety-first hierarchy [3].

The main reason for this brittleness is the difficulty of simultaneously satisfying diverse constraints, which requires suitable prioritization. A principled approach to such prioritization is seen in planning with formal methods, where logical specifications capture safety guarantees. Examples include optimizing the satisfaction of Signal Temporal Logic formulas in a receding horizon framework [9, 26], and the synthesis of policies that maximize the probability of satisfying objectives given as Linear Temporal Logic predicates [16]. However, formal methods tools, in general, can lead to performance bottlenecks and lack in scalability [22, 28].

A more scalable technique to achieve prioritization is to adopt constrained optimization, where inviolable rules of the road [1] would be encoded as hard (in)equality constraints while secondary objectives are satisfied in a soft manner as dictated by weights in a cost function. In [27], planning is formulated in this way as a nonlinear constrained optimization problem in a Model Predictive Control (MPC) scheme,

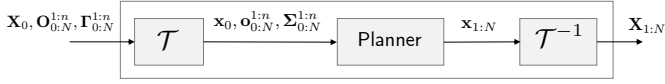


Fig. 2: From initial poses and covariances $(\mathbf{X}_0, \mathbf{O}_{0:N}^{1:n}, \mathbf{\Gamma}_{0:N}^{1:n})$, a transform \mathcal{T} yields the planner’s input in the reference path representation. The planner’s output is then projected back by \mathcal{T}^{-1} to a trajectory $\mathbf{X}_{1:N}$ in the global coordinate frame.

producing safe and smooth trajectories when it converges. However, as the authors note, there are several challenges with this approach, including the uncertain convergence and/or locally-optimal solutions, even when using state of the art, off-the-shelf solvers [27].

We propose a two-stage optimization method that preserves prioritization of objectives without compromising convergence and optimality. Specifically, we pose the problem in terms of a first stage modeled as a Mixed-Integer Linear Program (MILP), the output of which is seeded to a Nonlinear Programming (NLP) problem. The informed initialization offered by the first stage is an approximate solution that is globally ε -optimal [13, 23] up to a user-defined receding horizon. This facilitates for the subsequent nonlinear constrained optimization to produce a safe, smooth and feasible trajectory.

Contributions Our contributions are twofold:

- 1) we formulate motion planning for autonomous driving in a two-stage optimization framework, and
- 2) we evaluate the framework thoroughly in a range of simulated complex driving situations to demonstrate that our approach leads to a higher percentage of solved examples and more comfortable, yet assertive, solutions.

II. PRELIMINARIES AND PROBLEM STATEMENT

A. Notation and Definitions

We use the shorthand $k \equiv t_k = t_0 + k\Delta t$, where t_0 is current time and Δt the timestep. We assume the planning problem to be defined over N steps with a temporal horizon of $\tau = N\Delta t$. For any variable r_j with $j \in \mathbb{N}^+$, we use the shorthand notation $r_{i:e} \equiv (r_i, \dots, r_e)$. Vectors are in bold.

We refer to the vehicle whose motion we want to plan as the *ego-vehicle* and consider its state at time k to be given by $\mathbf{X}_k = (X_k, Y_k, \Phi_k, V_k) \in \mathcal{W}_X$, where (X_k, Y_k) is the position, Φ_k is its heading, and V_k is its speed, all in a global coordinate frame \mathcal{W} . The ego state at time 0 is given by \mathbf{X}_0 , while the output of planning is the vector of ego states over the next N steps, $\mathbf{X}_{1:N} \in \mathcal{W}_X^N$.

Other traffic participants, such as vehicles, pedestrians and cyclists, are indexed by $i \in \{1, \dots, n\}$, and their mean pose at time k is $\mathbf{O}_k^i = (X_k^i, Y_k^i, \Phi_k^i) \in \mathcal{W}_O$. Uncertainty over their positions is modeled by a Gaussian distribution with mean (X_k^i, Y_k^i) and covariance $\mathbf{\Gamma}_k^i$. The set of the mean poses of all traffic participants over the planning horizon $\mathbf{O}_{0:N}^{1:n}$ and the covariances $\mathbf{\Gamma}_{0:N}^{1:n}$ are inputs to the planning problem.

We assume the planning goal to be defined as continuous progress along a differentiable and bounded two-dimensional reference path, \mathcal{P}_{ref} , of length $|\mathcal{P}_{\text{ref}}|$, parameterized by the distance from its start, $\lambda \in [0, |\mathcal{P}_{\text{ref}}|]$, as $(X^{\mathcal{P}_{\text{ref}}}(\lambda), Y^{\mathcal{P}_{\text{ref}}}(\lambda))$.

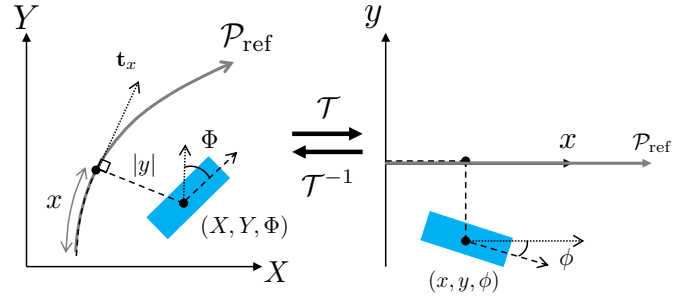


Fig. 3: Visual representation of the pose transform of \mathcal{T} between the world frame of reference (left) and the reference path based frame (right), and \mathcal{T}^{-1} , the inverse transform.

To simplify the planning problem, we transform the global coordinate frame \mathcal{W} to a \mathcal{P}_{ref} -based representation \mathcal{W}_r under the invertible transform \mathcal{T} , as presented in the next section. Fig. 2 illustrates the process of going from an input $(\mathbf{X}_0, \mathbf{O}_{0:N}^{1:n}, \mathbf{\Gamma}_{0:N}^{1:n})$ to the desired planning output $\mathbf{X}_{1:N}$.

B. Reference Path Representation

Given the definition of the reference path \mathcal{P}_{ref} , we can write:

$$\mathbf{t}_\lambda = \begin{bmatrix} \frac{\partial X^{\mathcal{P}_{\text{ref}}}(\lambda)}{\partial \lambda} \\ \frac{\partial Y^{\mathcal{P}_{\text{ref}}}(\lambda)}{\partial \lambda} \end{bmatrix}, \quad \mathbf{n}_\lambda = \begin{bmatrix} -\frac{\partial Y^{\mathcal{P}_{\text{ref}}}(\lambda)}{\partial \lambda} \\ \frac{\partial X^{\mathcal{P}_{\text{ref}}}(\lambda)}{\partial \lambda} \end{bmatrix} \quad (1)$$

where \mathbf{t}_λ and \mathbf{n}_λ are the tangential and normal vectors of the reference path in the global coordinate frame.

The invertible transform \mathcal{T} operates on the input of the planning problem: (1) *poses*, (2) *velocities* and (3) *covariance matrices*:¹

1) *Pose transform*: \mathcal{T} maps the pose (X, Y, Φ) in the global coordinate frame \mathcal{W} to pose (x, y, ϕ) in the reference path frame \mathcal{W}_r , as presented in Fig. 3.

- $x = \text{proj}_{\mathcal{P}_{\text{ref}}}[X \ Y]$ is the distance λ from the beginning of \mathcal{P}_{ref} to the projection of $[X \ Y]$ into it, defined as:

$$x = \underset{\lambda}{\text{argmin}} \quad (X - X^{\mathcal{P}_{\text{ref}}}(\lambda))^2 + (Y - Y^{\mathcal{P}_{\text{ref}}}(\lambda))^2.$$

Due to the nature of the optimization, no closed-form solution can be obtained for x .

- $y = \frac{1}{\|\mathbf{n}_x\|} \mathbf{n}_x^T \cdot \hat{\mathbf{y}}$, where \mathbf{n}_x is the normal vector of the reference path at $\lambda = x$ as in (1), and $\hat{\mathbf{y}} = \begin{bmatrix} X - X^{\mathcal{P}_{\text{ref}}}(x) \\ Y - Y^{\mathcal{P}_{\text{ref}}}(x) \end{bmatrix}$.
- $\phi = \angle \mathbf{t}_x - \Phi$, where:

$$\angle \mathbf{t}_x = \arctan \left(\left. \frac{\partial Y^{\mathcal{P}_{\text{ref}}}(\lambda)}{\partial X^{\mathcal{P}_{\text{ref}}}(\lambda)} \right|_{\lambda=x} \right). \quad (2)$$

2) *Velocity transform*: \mathcal{T} is a spatial transformation, so speeds are invariant: $v = \mathcal{T}(V) = V$.

3) *Covariance transform*: considering a traffic participant with pose \mathbf{O} and covariance $\mathbf{\Gamma}$, $\mathcal{T}(\mathbf{O}) = [x \ y \ \phi]^T$, the transformed covariance matrix is given by:

$$\mathbf{\Sigma} = \mathcal{T}(\mathbf{\Gamma}) = R(\angle \mathbf{t}_x - \phi) \mathbf{\Gamma} R(\angle \mathbf{t}_x - \phi)^T \quad (3)$$

where $\angle \mathbf{t}_x$ is as defined in (2), and $R(\varphi) \in SO(2)$ is the rotation matrix for angle φ .

¹The derivation of \mathcal{T}^{-1} is similar to \mathcal{T} , and thus is omitted.

C. Problem Statement

The planning problem is defined in the reference path coordinate frame. The state of the ego-vehicle at time k is given by $\mathbf{x}_k = (x_k, y_k, \phi_k, v_k) \in \mathcal{X}$ where (x_k, y_k) is the position, ϕ_k is its heading, and v_k is its speed. The evolution of the state is given by a discrete general dynamical system:

$$\mathbf{x}_{k+1} = f_{\Delta t}(\mathbf{x}_k, \mathbf{u}_k), \quad (4)$$

where $f_{\Delta t}$ is a discrete, nonlinear function parameterized by Δt , and $\mathbf{u}_k = (a_k, \delta_k) \in \mathcal{U}$ is the acceleration and steering angle controls applied at time k . We consider the ego-vehicle to be a rigid body occupying an area $S_e \subset \mathbb{R}^2$ relative to its center, and denote the area occupied by the ego-vehicle at state \mathbf{x}_k by $\mathcal{S}(\mathbf{x}_k) \subset \mathbb{R}^2$.

For other traffic participants $i \in \{1, \dots, n\}$, pose at time k is given by $\mathbf{o}_k^i = (x_k^i, y_k^i, \phi_k^i) \in \mathcal{O}$ and position covariance by Σ_k^i . Following the definition from [27], we denote the area each traffic participant occupies with probability higher than p_ϵ by $\mathcal{S}^i(\mathbf{o}_k^i, \Sigma_k^i, p_\epsilon) \subset \mathbb{R}^2$.

We define the driveable surface area $\mathcal{B} \subset \mathbb{R}^2$ to be the area in which it is safe for the ego-vehicle to drive in the reference path coordinate frame, and the unsafe area $\mathcal{B}_{out} = \mathbb{R}^2 \setminus \mathcal{B}$. With a cost function $J(\mathbf{x}_{0:N}, \mathbf{u}_{0:N-1})$ defined over the positions and controls of the ego-vehicle, we can now pose the problem.

Problem 1 (Motion Synthesis). Given an initial ego state \mathbf{x}_0 , and trajectories of other traffic participants $(\mathbf{o}_{0:N}^{1:n}, \Sigma_{0:N}^{1:n})$, compute:

$$\begin{aligned} \underset{\mathbf{x}_{1:N}, \mathbf{u}_{0:N-1}}{\operatorname{argmin}} \quad & J(\mathbf{x}_{0:N}, \mathbf{u}_{0:N-1}) \\ \text{s.t.} \quad & \forall k \in \{0, \dots, N\}: \\ & \mathbf{x}_{k+1} = f_{\Delta t}(\mathbf{x}_k, \mathbf{u}_k) \\ & \mathcal{S}(\mathbf{x}_k) \cap \mathcal{B}_{out} = \emptyset \\ & \mathcal{S}(\mathbf{x}_k) \cap \left[\bigcup_{i \in \{1, \dots, n\}} \mathcal{S}^i(\mathbf{o}_k^i, \Sigma_k^i, p_\epsilon) \right] = \emptyset \end{aligned}$$

III. NONLINEAR PROGRAMMING FORMULATION

In this section, we describe a specific solution method to Problem 1, posing it as an NLP problem comprising: (1) *kinematic vehicle model constraints* on the model transitions and allowed controls (Sec. III-1); (2) *collision avoidance constraints* with the boundaries of the driveable area as well as other traffic participants (Sec. III-2); and (3) *a multi-objective cost function* over soft constraints (Sec. III-3).

1) *Vehicle Model:* We consider a discrete kinematic bicycle model based on the center of the vehicle. Assuming the ego-vehicle to be a rectangle with an inter-axel distance L , we write:

$$\begin{bmatrix} x_{k+1} \\ y_{k+1} \\ \phi_{k+1} \\ v_{k+1} \end{bmatrix} = \begin{bmatrix} x_k \\ y_k \\ \phi_k \\ v_k \end{bmatrix} + \begin{bmatrix} v_k \cos(\phi_k + \delta_k) \\ v_k \sin(\phi_k + \delta_k) \\ \frac{2v_k}{L} \sin(\delta_k) \\ a_k \end{bmatrix} \Delta t \quad (5)$$

While the kinematic bicycle model is not strictly limited by any specific values of maximum steering or acceleration, we

impose the limits $|\delta_k| \leq \delta_{\max}$ and $a_{\min} \leq a_k \leq a_{\max}$, as well as limit jerk $|a_{k+1} - a_k| \leq \dot{a}_{\max}$ and angular jerk $|\delta_{k+1} - \delta_k| \leq \dot{\delta}_{\max}$ to stay within the operational domain and for passenger comfort. We also constrain speed, $0 \leq v_{\min} \leq v_k \leq v_{\max}$, to obtain forward motion within the set speed limit.

2) *Collision Avoidance:* We consider two different types of collision avoidance: the limits of the driveable surface (including road limits and roadworks) and other traffic participants (referred to as vehicles in this section for the sake of brevity). To define an adequate representation of the area of the ego-vehicle $\mathcal{S}(\mathbf{x}_k)$ given state \mathbf{x}_k , we relax the ego-vehicle boundary definition to its corners. For a rectangular vehicle of width w and length l , the positions of the corners at \mathbf{x}_k are:

$$\mathbf{c}^z(\mathbf{x}_k) = \begin{bmatrix} x_k^z \\ y_k^z \end{bmatrix} = R(\phi_k) \left(\mathbf{z}^T \circ \begin{bmatrix} w/2 \\ l/2 \end{bmatrix} \right) + \begin{bmatrix} x_k \\ y_k \end{bmatrix} \quad (6)$$

where $\mathbf{z} \in \mathcal{Z} = \{[1 \ 1], [-1 \ 1], [-1 \ -1], [1 \ -1]\}$, $R(\phi_k) \in SO(2)$ is the rotation matrix for angle ϕ_k , and \circ is the element-wise product.

With this, the driveable surface constraint $\mathcal{S}(\mathbf{x}_k) \cap \mathcal{B}_{out} = \emptyset$ can be reduced to:

$$\forall \mathbf{z} \in \mathcal{Z} : \mathbf{c}^z(\mathbf{x}_k) \in \mathcal{B}. \quad (7)$$

The driveable surface \mathcal{B} is described by two continuous and differentiable functions of x , the left border $b_l(x)$ and the right border $b_r(x)$, such that $\forall x : b_l(x) > b_r(x)$. These boundaries impose a constraint on y , the lateral path deviation at position x . Then, (7) can be reduced to the set of constraints

$$\forall \mathbf{z} \in \mathcal{Z} : b_l(x_k^z) \geq y_k^z \geq b_r(x_k^z), \quad (8)$$

with $[x_k^z, y_k^z]^T$ defined as in (6).

For collision avoidance with other vehicles, we model their area $\mathcal{S}^i(\mathbf{o}_k^i, \Sigma_k^i, p_\epsilon)$ in a similar fashion to [27]. Assuming $a_{\text{shape}}, b_{\text{shape}}$ to be the parameters of an ellipsis that inscribes the vehicle's shape, and Σ_k^i to be axis aligned with the vehicle's axis, we write:

$$S^i \subset \mathcal{L}(a_{\Sigma_k^i} + a_{\text{shape}}, b_{\Sigma_k^i} + b_{\text{shape}}) = \mathcal{L}(a_k^i, b_k^i) \quad (9)$$

where $\mathcal{L}(a_k^i, b_k^i)$ is an ellipse conservatively inscribing vehicle i at time k up to an uncertainty p_ϵ . For more details, see [27]. Thus, we write the constraints:

$$g^{i,z}(\mathbf{x}_k) > 1, \quad \forall \mathbf{z} \in \mathcal{Z}, \quad (10)$$

$$g^{i,z}(\mathbf{x}_k) = \begin{bmatrix} x_k^z - x_k^i \\ y_k^z - y_k^i \end{bmatrix}^T R(\phi_k^i)^T \begin{bmatrix} (a_k^i)^{-2} & 0 \\ 0 & (b_k^i)^{-2} \end{bmatrix} R(\phi_k^i) \begin{bmatrix} x_k^z - x_k^i \\ y_k^z - y_k^i \end{bmatrix}$$

3) *Cost function:* A multi-objective cost function is defined over a set of soft constraints \mathcal{I} on the ego-vehicle's states and controls. For a soft constraint $\iota \in \mathcal{I}$: $\theta_\iota(\mathbf{x}, \mathbf{u})$ and weight $\omega_\iota \in \mathbb{R}^+$ reflecting its relative importance, the cost function can be defined as:

$$J(\mathbf{x}_{0:N}, \mathbf{u}_{0:N-1}) = \sum_{k=0}^N \sum_{\iota \in \mathcal{I}} \omega_\iota \theta_\iota(\mathbf{x}_k, \mathbf{u}_k) \quad (11)$$

Soft constraints are defined over different objectives:

- **Progress** towards a longitudinal goal x_g : $\theta_x = (x - x_g)^2$, a target speed v_g : $\theta_v = (v - v_g)^2$, and for lateral tracking of the reference path, $\theta_y = y^2$.
- **Comfort** as a minimization of the norm of acceleration, $\theta_a = a^2$, and steering, $\theta_\delta = \delta^2$.

4) *NLP formulation*: We formulate the optimization problem using the constraints previously defined.

Problem 2 (Nonlinear Programming Problem). Given an initial ego-vehicle state \mathbf{x}_0 , trajectories of traffic participants $(\mathbf{o}_{0:N}^{1:n}, \Sigma_{0:N}^{1:n})$ and soft constraints \mathcal{I} , compute:

$$\begin{aligned} \underset{\mathbf{x}_{1:N}, \mathbf{u}_{0:N-1}}{\operatorname{argmin}} \quad & \sum_{k=0}^N \sum_{\ell \in \mathcal{I}} \omega_\ell \theta_\ell(\mathbf{x}_k, \mathbf{u}_k) \\ \text{s.t.} \quad & \forall k \in \{0, \dots, N\} : \\ & \mathbf{x}_{k+1} = f_{\Delta t}(\mathbf{x}_k, \mathbf{u}_k) \\ & |\delta_k| \leq \delta_{\max} \\ & a_{\min} \leq a_k \leq a_{\max} \\ & |a_{k+1} - a_k| \leq \dot{a}_{\max} \\ & |\delta_{k+1} - \delta_k| \leq \dot{\delta}_{\max} \\ & v_{\min} \leq v_k \leq v_{\max} \\ & b_l(x_k^z) \geq y_k^z \geq b_r(x_k^z), \mathbf{z} \in \mathcal{Z} \\ & g^{i,z}(\mathbf{x}_k) > 1, i \in \{1, \dots, n\}, \mathbf{z} \in \mathcal{Z} \end{aligned}$$

Due to the nonlinearity of J , $f_{\Delta t}$, b_l , b_r and $g^{i,z}$, this is a nonlinear, non-convex, constrained optimization problem with equality and inequality constraints. While it is appealing to solve the problem directly or using a receding horizon formulation as in [27], there are two major challenges:

- **Uncertain convergence**: solvers for this type of problems are generally slow for large instances, particularly when initialization is not carefully considered [24]. While advances in efficient primal-dual interior point solvers have mitigated this issue to a certain degree [8, 30, 10], the convergence to a solution is uncertain [27, 24, 12].
- **Local optima**: nonlinear constrained optimization solvers tend to be local in nature, finding solutions close to the initial point and, possibly, far from the global optimum [27, 13, 24].

IV. TWO-STAGE OPTIMIZATION

To mitigate the aforementioned issues of NLP, we propose the framework presented in Fig. 4. The main motivation behind the architecture is to avoid the local optima convergence in the nonlinear, non-convex constrained optimization by providing an informed initial solution that is closer to the global optimum, leading to faster and more reliable convergence.

In our two-stage optimization, the first stage solves a *linearized* version of Problem 2 in a finite, receding horizon manner using a Mixed-Integer Linear Programming formulation (details presented in Sec. IV-A). This gives optimality guarantees for each step of the receding horizon problem (see Sec. IV-A5), acting as a proxy toward reaching the global optimum of the linearized problem. The second stage solves

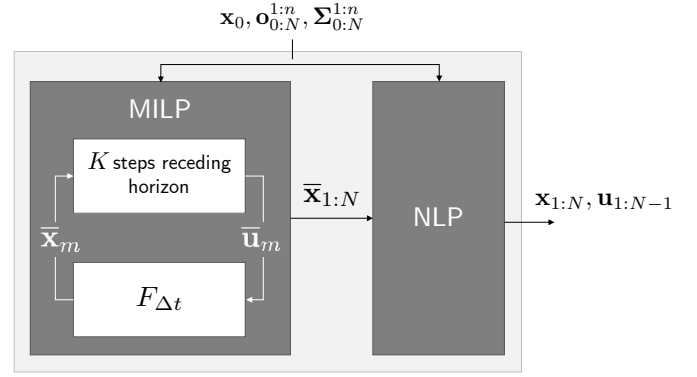


Fig. 4: *Two-stage architecture*: the first stage (left) solves a receding horizon formulation of a linearized version of the problem; the second stage (right) uses the solution of the first stage as initialization to solve the full nonlinear, non-convex, constrained optimization problem.

Problem 2 using the output of the MILP optimizer as an initialization. With similar representations of the linearized and nonlinear problems, the initialization should improve convergence, speed and the quality of the final solution.

A. Mixed-Integer Linear Programming Formulation

In this section, we reformulate Problem 2 as a MILP problem. To do so, we consider a linear vehicle model with kinematic feasibility constraints, an approach to collision avoidance which maintains the mixed-integer linearity of the model, and adapt the soft constraints to a MILP cost function. Then, we define the full problem and discuss solution optimality. We make use of the nonlinear operators $|\cdot|$ and $\max(\cdot)$, which we enforce through auxiliary binary variables under the *big-M* formulation [32, 25].

1) *Linear Vehicle Model and Kinematic Feasibility*: The kinematic bicycle model presented in Sec. III-1 is nonlinear, but can be linearized around a point using a series expansion. The problem with this approach lies on the fact that this approximation is only valid around the point, yielding higher errors as the distance to the point increases. To avoid this issue, we consider a nonholonomic vehicle model. We define a state of this linear vehicle model at time k as $\bar{\mathbf{x}}_k = [x_k \ y_k \ v_k^x \ v_k^y] \in \mathcal{X}^{\mathcal{M}}$, where

$$v_k^x = v_k \cos(\phi_k), \quad v_k^y = v_k \sin(\phi_k) \quad (12)$$

with controls $\bar{\mathbf{u}}_k = [a_k^x \ a_k^y] \in \mathcal{U}^{\mathcal{M}}$, and consider a linear vehicle dynamics model defined as:

$$\bar{\mathbf{x}}_{k+1} = F_{\Delta t}(\bar{\mathbf{x}}_k, \bar{\mathbf{u}}_k) = A_d \bar{\mathbf{x}}_k + B_d \bar{\mathbf{u}}_k \quad (13)$$

where $F_{\Delta t}$ corresponds to a zero-order hold discretization of the continuous state-space system:

$$\dot{\bar{\mathbf{x}}} = \begin{bmatrix} 0 & 0 & 1 & 0 \\ 0 & 0 & 0 & 1 \\ 0 & 0 & 0 & 0 \\ 0 & 0 & 0 & 0 \end{bmatrix} \bar{\mathbf{x}}^T + \begin{bmatrix} 0 & 0 \\ 0 & 0 \\ 1 & 0 \\ 0 & 1 \end{bmatrix} \bar{\mathbf{u}}^T \quad (14)$$

This nonholonomic model is highly simplified when compared to the kinematic bicycle model in (5). To induce kinematic feasibility, we add the constraint:

$$v^x \geq \rho |v^y| \quad (15)$$

for a constant $\rho \in \mathbb{R}^+$. Assuming forward motion, that is $\phi_k \in [-\frac{\pi}{2}, \frac{\pi}{2}]$, this constraint dictates that any movement in the y direction requires motion in the x direction as well.

We also enforce the same constraints as in the nonlinear model, in particular input bound constraints, $a_{\min}^x \leq a_k^x \leq a_{\max}^x$ and $a_{\min}^y \leq a_k^y \leq a_{\max}^y$; jerk constraints, $|a_{k+1}^x - a_k^x| < \Delta a_{\max}^x \Delta t$ and $|a_{k+1}^y - a_k^y| < \Delta a_{\max}^y \Delta t$; and velocity constraints $v_{\min}^x \leq v_k^x \leq v_{\max}^x$ and $v_{\min}^y \leq v_k^y \leq v_{\max}^y$, with $v_{\min}^x \geq 0$ to guarantee forward motion.

2) *Collision Avoidance*: Similarly to the nonlinear formulation, collision avoidance is split into avoiding the limits of the driveable surface and other traffic participants. A key difference though is the lack of explicit representation of orientation in the state $\bar{\mathbf{x}}$, so that a linear approximation of the ego-vehicle's corners would induce large errors in the model. We instead consider the ego-vehicle to be a point and leave handling the area it occupies to the definition of the limits of the driveable surface and other traffic participants.

For the driveable surface, we define piecewise-linear functions for the left and right road boundaries $b_l^M(x)$ and $b_r^M(x)$, such that $\forall x : b_l^M(x) > b_r^M(x)$. To take the size of the ego-vehicle into account, we formulate the constraint:

$$d + b_l^M(x_k) \geq y_k \geq b_r^M(x_k) - d \quad (16)$$

where $d : \mathcal{S}_e \rightarrow \mathbb{R}$ is a function of the shape of the ego-vehicle. In the most conservative case assuming a rectangular shape with width w and length l , we can define $d = \sqrt{(w^2 + l^2)}/2$, i.e. restrict the driveable surface to $\mathcal{B} = \mathbb{R}^2 \setminus (\mathcal{B}_{out} \oplus \mathcal{S}_e)$ where \oplus is the Minkowski-sum operator. For practical purposes, we consider $d = w/2$, which is exact when $\phi = 0$.

For traffic participants, we inscribe the ellipses $\mathcal{L}(a_k^i, b_k^i)$ defined in (9) with axis-aligned rectangles, augmented to consider the shape of the ego-vehicle. With d^x and d^y being functions of the size of the ego-vehicle with respect to its center in the x and y direction, respectively, we define rectangles \mathcal{R}_k^i with the limits:

$$\begin{aligned} x_{k,\min}^i &= \left[\min_x \mathcal{L}(a_k^i, b_k^i) \right] - d^x \\ x_{k,\max}^i &= \left[\max_x \mathcal{L}(a_k^i, b_k^i) \right] + d^x \\ y_{k,\min}^i &= \left[\min_y \mathcal{L}(a_k^i, b_k^i) \right] - d^y \\ y_{k,\max}^i &= \left[\max_y \mathcal{L}(a_k^i, b_k^i) \right] + d^y. \end{aligned} \quad (17)$$

It should be noted that $x_{k,\min}^i, x_{k,\max}^i, y_{k,\min}^i, y_{k,\max}^i$ can be computed in closed form from $\mathcal{L}(a_k^i, b_k^i)$, d_x and d_y . Then, the collision avoidance constraint is the logical implication:

$$(x_{k,\min}^i \leq x \leq x_{k,\max}^i \wedge y \geq y_{k,\min}^i) \Rightarrow y \geq y_{k,\max}^i \quad (18)$$

which reads *if the ego's position is aligned with a vehicle along x , then it must be outside the vehicle's borders in y* . Using the *big-M* formulation [32, 25] with a sufficiently large $M \in \mathbb{R}^+$, we get the following mixed-integer constraint:

$$\begin{aligned} y_{k,\max}^i - M\mu_k^i &\leq y_k \text{ where} \\ \mu_k^i &= \max(x_{k,\min}^i - x_k, 0) + \max(x_k - x_{k,\max}^i, 0) \\ &\quad + \max(y_{k,\min}^i - y_k, 0) \end{aligned} \quad (19)$$

3) *Mixed-Integer Linear Cost Function*: It is imperative that the MILP cost function be similar to the one from the nonlinear stage in order to minimize the gap between the optimum of the two stages. Since we are defining the problem in a receding horizon formulation, the cost over each state is also defined independently in time, as, for $k \in \{0, \dots, N\}$:

$$J_C^{\mathcal{M},k}(\bar{\mathbf{x}}, \bar{\mathbf{u}}) = \sum_{\iota \in \mathcal{C}} \Omega_\iota \Theta_\iota(\bar{\mathbf{x}}, \bar{\mathbf{u}}), \quad (20)$$

for a set of soft constraints \mathcal{C} , where each constraint ι is a function $\Theta_\iota(\bar{\mathbf{x}}, \bar{\mathbf{u}})$ with a weight $\Omega_\iota \in \mathbb{R}^+$. The weights determine the relative importance of each constraint and require fine tuning. Similarly to the nonlinear stage, soft constraints are defined over different objectives:

- **Progress** towards a longitudinal goal x_g , $\Theta_x = |x - x_g|$; a target speed v_g , $\Theta_v = |v - v_g|$; and over lateral tracking of the reference path, $\Theta_y = |y|$.
- **Comfort** as a minimization of the norm of lateral acceleration, $\Theta_a = |a_y|$.

4) *MILP Problem Definition*: With constraints \mathcal{C} and cost function $J^{\mathcal{M},k}$, we formulate the problem as a K -step receding horizon MILP one. In the end, we obtain $\bar{\mathbf{x}}_{1:N}$.

Problem 3 (Receding Horizon MILP). Given an initial ego-vehicle state $\bar{\mathbf{x}}_0$, trajectories of other traffic participants $(\mathbf{O}_{0:N}^{1:n}, \mathbf{\Sigma}_{0:N}^{1:n})$, a set of soft constraints \mathcal{C} , and a planning step $0 \leq m \leq N - K$ of the receding horizon, compute:

$$\begin{aligned} \underset{\bar{\mathbf{x}}_{m+1:m+K}, \bar{\mathbf{u}}_{m:m+K-1}}{\text{argmin}} \quad & \sum_{k=m}^{m+K} \sum_{\iota \in \mathcal{C}} \Omega_\iota \Theta_\iota(\bar{\mathbf{x}}_k, \bar{\mathbf{u}}_k) \\ \text{s.t.} \quad & \forall k \in \{m, \dots, m+K\} : \\ & \bar{\mathbf{x}}_{k+1} = F_{\Delta t}(\bar{\mathbf{x}}_k, \bar{\mathbf{u}}_k) \\ & a_{\min}^x \leq a_k^x \leq a_{\max}^x \\ & a_{\min}^y \leq a_k^y \leq a_{\max}^y \\ & |a_{k+1}^x - a_k^x| < \Delta a_{\max}^x \Delta t \\ & |a_{k+1}^y - a_k^y| < \Delta a_{\max}^y \Delta t \\ & v_{\min}^x \leq v_k^x \leq v_{\max}^x \\ & v_{\min}^y \leq v_k^y \leq v_{\max}^y \\ & v^x \geq \rho |v^y| \\ & d + b_l^M(x_k) \geq y_k \\ & y_k \geq b_r^M(x_k) - d \\ & y_{k,\max}^i - M\mu_k^i \leq y_k, i \in \{1, \dots, n\} \end{aligned}$$

5) *On the optimality of the MILP formulation:* The final optimal solution of Problem 3 acts as the initial solution to Problem 2 in order to tackle uncertain convergence and local optima challenges that arise from solving the NLP directly. A solution to Problem 3 can be obtained using Branch and Bound, a divide and conquer algorithm first introduced and applied to MILP solving by Land and Doig [20]. This solution is proven to be the global ε -optimal one [13, 23]. In practice, modern solvers (e.g. Gurobi or CPLEX) may fail to find the global solution due to rounding errors and built-in tolerances [23]. On top of this, the receding horizon formulation of the problem, introduced for the sake of computational tractability, generates suboptimality by definition [11, 14]. Due to these factors, no strong theoretical guarantee can be given regarding the solution of the MILP stage.

Despite this, a solution that is close to the global optimum at each receding horizon step acts as a proxy towards a final solution that is close to the global optimum and, in turn, initializing the NLP stage using this output could improve the quality of the solution at that stage. In general, our experiments corroborate this hypothesis.

V. RESULTS AND EVALUATION

In this section, we will show that:

- 1) our method is general and can be applied to a diversity of driving situations;
- 2) the MILP stage provides the NLP stage with a better initialization when compared to simpler heuristics, leading to a higher percentage of solved cases, faster NLP solving times and solutions closer to the global optimum; and
- 3) our method leads to solutions that outperform a Nonlinear Model Predictive Control (NMPC) approach similar to the one presented in [27] in progress and comfort metrics.

To that end, we implement the first stage (MILP; Problem 3) using Gurobi 8.1 [15], and the second stage (NLP; Problem 2) using IPOPT [31]. Both solvers have a timeout of 25s, after which the optimization is stopped. We use $N = 40$ and $\Delta t = 0.2s$ for a trajectory horizon of $8s$.² Without loss of generality, we assume *left-hand traffic* where drivers are expected to be on the left hand side of the road, that a route planner is available to generate a reference path that satisfies the planning goal in the global coordinate frame, and consider a constant velocity model for the prediction of dynamic agents. In the simulator, the behavior of other dynamic vehicles is based on the Intelligent Driver Model [29].

1) **Generality:** Figures 5 and 6 show two qualitatively distinct driving situations. In Figure 5 the ego-vehicle overtakes parked vehicles on a two-lane road while taking into account an oncoming vehicle on the other lane that is also overtaking a static vehicle in its own lane. The plots in Figure 5d show the ego deviating from its own lane (the reference path) for overtaking, and returning to it as soon as possible, while

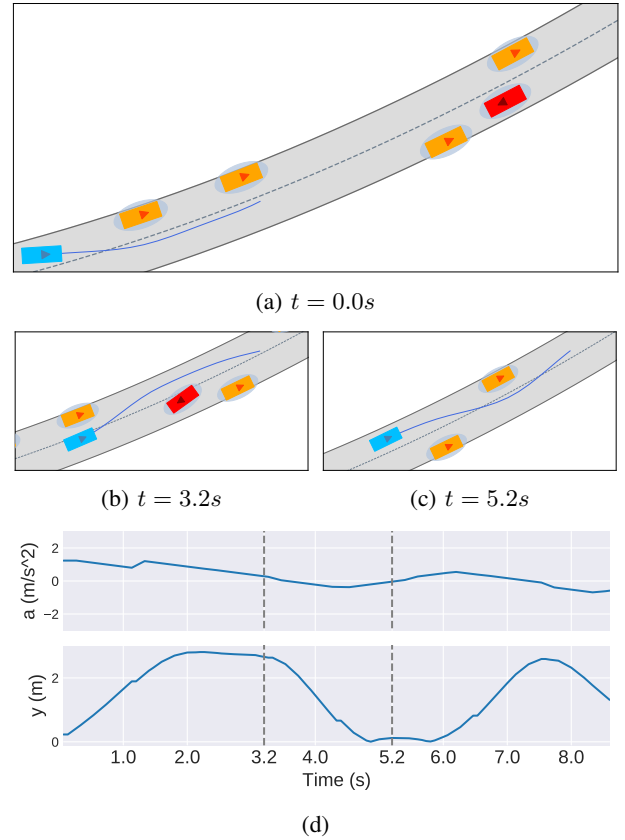


Fig. 5: *Residential Driving - Static Overtaking with Oncoming Vehicle:* navigation of a residential driving example, presented in the top of Figure 1. (a), (b), (c): top down view of the situation at timestep t , with the ego in blue, static obstacles in orange and an oncoming vehicle in red; the ego’s plan at time t is in dark blue. (d) plots of the acceleration profile used and lateral deviation from the reference path.

always maintaining a smooth acceleration profile. The second example in Figure 6 shows an *unprotected* right-turn into a main road. Figure 6d shows the ego-vehicle closely follows the reference path (right turn into the main road) while smoothly responding to unforeseen behaviors of the dynamic vehicles.

Figure 7 shows examples of the four different simulation *scenarios* we consider for experiments 2) and 3): (SO) static overtaking of parked vehicles on both sides of the road; (SO+OV) static overtaking with a dynamic vehicle in the oncoming lane; (DO) dynamic overtaking of a slow moving vehicle; and (DO+OV) dynamic overtaking with an oncoming vehicle on the other lane. For the experiments, we generate datasets of *examples* per scenario by randomizing over relevant parameters (e.g. initial speeds and number of vehicles). More details are presented in Appendix B.

2) **Initialization Comparison:** We consider four heuristic initializations as alternatives to our MILP stage: ZEROS, in which all states and controls are initialized to zero; C.VEL, where the ego-vehicle is assumed to maintain its speed throughout the solution; C.ACC, where the ego-vehicle main-

²Other parameters are listed in Appendix A

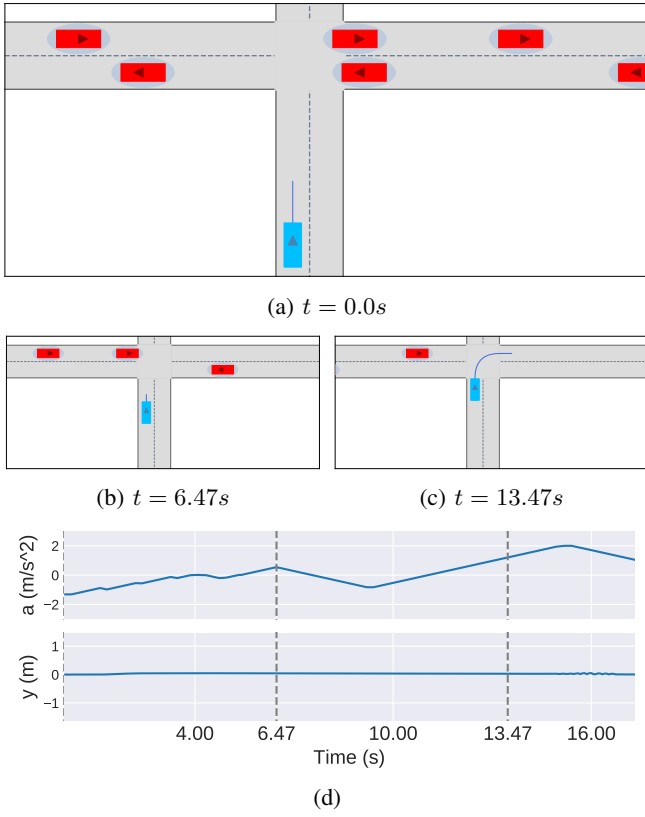


Fig. 6: *Junction - Unprotected Right Turn*: navigation of a junction example, presented in the bottom of Figure 1. (a), (b), (c): top down view of the situation at timestep t , with the ego in blue, and dynamic vehicles in red; the ego’s plan at time t is in dark blue. (d) plots of the acceleration profile used and lateral deviation from the reference path.

	SO	SO+OV	DO	DO+OV
ZEROS	98.57%	95.55%	96.97%	93.48%
C.VEL	96.85%	85.68%	42.42%	32.40%
C.ACC	89.23%	64.43%	5.61%	1.97%
C.DEC	98.58%	95.66%	88.79%	92.44%
Ours	98.47%	95.77%	99.40%	98.14%

TABLE I: *Initialization Comparison*: percentage of solved examples per initialization (rows) and scenario (columns).

tains a constant acceleration of $1ms^{-2}$ until the maximum speed is achieved; and C.DEC where the ego-vehicle maintains a constant acceleration of $-1ms^{-2}$ until it stops.

A dataset of 1000 examples per scenario was procedurally generated, solved using our method as well as using only the NLP stage for the same constrains initialized by each of the four heuristics. Table I presents the percentage of solved examples within the allocated time (25s) per initialization method and scenario. As it can be observed, our method either performs similarly or outperforms other methods in all the scenarios considered. In Figure 8, we analyze the problems that were solved using our initialization when compared to the other initialization methods. We observe that, across scenarios,

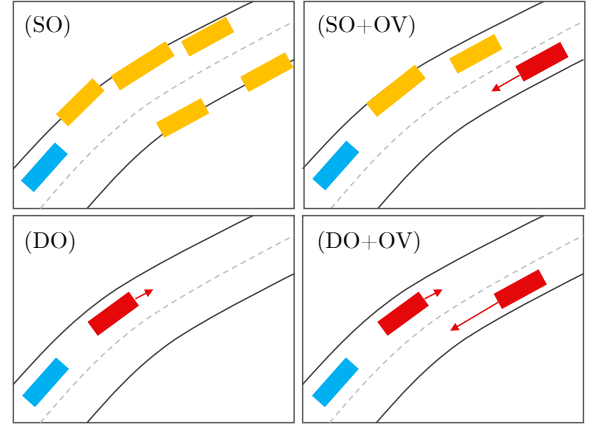


Fig. 7: *Residential Driving Scenarios*: with static vehicles are in yellow and dynamic agents in red, (SO) static overtaking of parked vehicles, (SO+OV) static overtaking with an oncoming vehicle in the other lane, (DO) dynamic overtaking of a slow moving vehicle, (DO+OV) dynamic overtaking of a slow moving vehicle with an oncoming vehicle in the other lane.

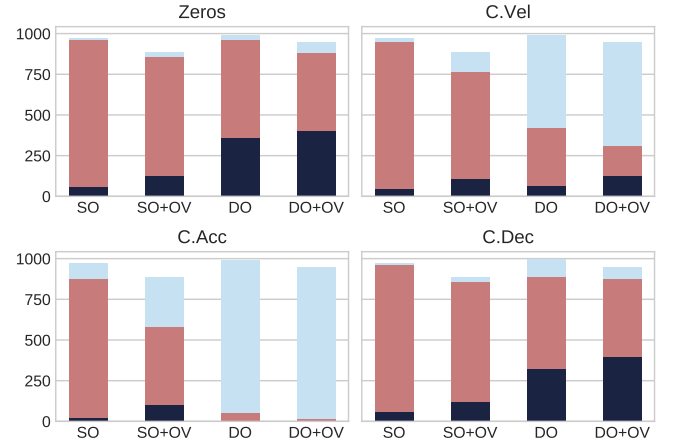


Fig. 8: *Initialization Comparison*: each plot corresponds to a different initialization, and each bar to a certain scenario; in light blue (top bar) are the problems solved by our method but not by the alternative initialization; in pink (middle bar) are the problems where the same solution is reached; in dark blue (bottom bar) are the problems where solutions differed.

ZEROS and C.DEC lead to the highest percentage of solved problems (after ours) and same solutions, but also the highest percentage of different solutions. To analyze this further, for problems where a different solution is reached (dark blue bars in Figure 8) Table II shows the average % difference in cost that the alternatives achieve compared to ours. For problems with similar solutions (pink bars in Figure 8), Table II presents the average % difference in the solving time of the NLP stage.

We see that, in general, other initialization methods obtain higher costs on average than ours. While C.ACC is able to achieve a lower average cost in some scenarios, it leads to a substantial number of unsolved examples, particularly for DO and DO+OV (see Figure 8). In all scenarios where the same

Init.	% Change in Cost (# situations)				% Change in Solving Time (# situations)			
	SO	SO+OV	DO	DO+OV	SO	SO+OV	DO	DO+OV
ZEROS	+85.39(56)	+68.53(126)	+52.36(356)	+25.96(403)	+42.86(902)	+47.62(728)	+154.42(607)	+104.44(483)
C.VEL	+60.24(44)	+47.69(112)	+29.55(64)	+1.35(126)	+12.53(903)	+16.39(652)	+70.01(358)	+94.71(187)
C.ACC	+6.16(20)	-10.77(100)	+0.01(2)	-7.67(5)	+12.93(856)	+19.16(478)	+231.79(54)	+306.32(14)
C.DEC	+85.01(55)	+67.39(123)	+36.79(322)	+24.51(396)	+7.93(903)	+3.43(732)	+70.23(565)	+17.61(483)

TABLE II: *Initialization Comparison*: in cases where the optimum is different (left), the average percent difference in the objective function value (cost) between the alternative method and our solution is shown (positive and higher is better for our method), with the respective number of examples in parenthesis; in cases in which the optimum is the same (right), the average difference in solving time as a percentage of the solving time of the NLP stage of our method is shown (positive and higher is better for our method), with the number of examples in parenthesis.

solution is reached by an alternative method, it takes longer to solve on average. A noteworthy case is DO+OV initialized with C.ACC which takes 306.32% longer on average to reach the same solution as ours. These results validate our claim that we achieve a higher percentage of solved examples (as shown by Table I), faster solving times and more optimal solutions (as evidenced by Figure 8 and Table II).

3) *NMPC Baseline Comparison*: We compare our method to an NMPC baseline which optimizes Problem 2 with the same soft and hard constraint but in a receding horizon fashion similar to [27]. This baseline uses the same interior-point optimization method as our NLP stage to solve each of the horizon steps. To evaluate the quality of the methods, we introduce the following metrics that compare our solution, $(\mathbf{x}_{1:N}^{\text{Ours}}, \mathbf{u}_{1:N-1}^{\text{Ours}})$, to the baseline's, $(\mathbf{x}_{1:N}^{\text{NMPC}}, \mathbf{u}_{1:N-1}^{\text{NMPC}})$:

- *Progress*: our overall progress compared to the baseline's

$$\Delta P = \max(x_{1:N}^{\text{Ours}}) - \max(x_{1:N}^{\text{NMPC}})$$

- *Reference path deviation*: our average deviation from the reference path compared to the baseline's

$$\Delta D = \frac{1}{N-1} \sum_{k=1}^N |y_k^{\text{NMPC}}| - |y_k^{\text{Ours}}|$$

- *Target speed matching*: for a given target speed v_g , comparison of our average matching with the baseline's

$$\Delta v_M = \frac{1}{N-1} \sum_{k=1}^N |v_k^{\text{NMPC}} - v_g| - |v_k^{\text{Ours}} - v_g|$$

- *Jerk*: comparison of our average jerk value with the baseline's

$$\Delta |\dot{a}| = \frac{1}{N} \sum_{k=1}^N \frac{|a_k^{\text{NMPC}} - a_{k-1}^{\text{NMPC}}|}{\Delta t} - \frac{|a_k^{\text{Ours}} - a_{k-1}^{\text{Ours}}|}{\Delta t}$$

We generate 1000 examples per scenario and solve them using our method and the NMPC baseline. The top of Table III shows the percentage of examples solved by the methods. Our method solves more examples than the baseline in all scenarios. For the problems that are solved by both we show solution metrics per scenario in the bottom of Table III. We achieve significantly higher progress and better velocity matching across scenarios, and similar or slightly smaller jerk values and deviation from the reference path. This validate our

		SO	SO+OV	DO	DO+OV
% Solved	NMPC	96.15%	79.45%	89.17%	85.74%
	Ours	98.38%	96.50%	99.60%	98.65%
Metrics	ΔP (m)	7.12	8.37	4.63	8.04
	ΔD (m)	-0.03	0.06	0.10	0.03
	Δv_M ($\frac{m}{s}$)	0.81	0.79	0.25	0.49
	$\Delta \dot{a} $ ($\frac{m}{s^3}$)	0.01	0.01	0.01	0.0

TABLE III: *NMPC Baseline Comparison*: *Top* – percentage of solved examples per scenario. *Bottom* – average results for difference in progress ΔP , deviation from reference ΔD , velocity matching Δv_M , and jerk $\Delta |\dot{a}|$ (positive and higher is better).

claim that our method is better in progress and comfort metrics than the baseline that has a similar formulation to [27].

While our MILP stage improves the overall solutions, our two-stage method, using off-the-shelf solvers, takes up to 1s in $\sim 87.5\%$ of the examples presented in the results. One direction of future work is to investigate methods that would make the current framework more suitable for real-time [5].

Note that some of the examples in the datasets were not solvable by any of the methods due to our specific choice of hard constraints. For instance, while the vehicle dynamics would allow acceleration values as low as $-7ms^{-2}$, we limited the minimum acceleration to $-3ms^{-2}$ as a comfort constraint, rendering some randomly-generated examples unsolvable. A practical approach to deploy our framework in the real-world is to introduce multiple levels of hard constraints that differ in strictness while always maintaining safety.

VI. CONCLUSION

In this paper we introduced a two-stage optimization framework for autonomous driving which first solves a linearized version of the planning problem (formulated as MILP) to initialize the second nonlinear optimization stage. We show that our MILP initialization leads on average to a higher percentage of solved examples, lower costs, and better solving time for the NLP stage when compared to alternative initializations. Additionally, we show that the two-stage formulation solves more examples than an NMPC baseline, outperforming it in terms of progress and comfort metrics.

REFERENCES

- [1] Driving Standards Agency. *The Highway Code*. The Stationery Office, 2015.
- [2] Stefano V. Albrecht and Peter Stone. Autonomous agents modelling other agents: A comprehensive survey and open problems. *Artificial Intelligence*, 258:66–95, 2018.
- [3] Dario Amodei, Chris Olah, Jacob Steinhardt, Paul Christiano, John Schulman, and Dan Mané. Concrete problems in AI safety. *arXiv preprint arXiv:1606.06565*, 2016.
- [4] Edward Ayers, Francisco Eiras, Majd Hawasly, and Iain Whiteside. PaRoT: A practical framework for robust deep neural network training. *arXiv preprint arXiv:2001.02152*, 2020.
- [5] D Bertsimas and B Stellato. Online mixed-integer optimization in milliseconds. *Journal of Optimization Theory and Applications*, 183(2):490–519, 2019.
- [6] Alex Bewley, Jessica Rigley, Yuxuan Liu, Jeffrey Hawke, Richard Shen, Vinh-Dieu Lam, and Alex Kendall. Learning to drive from simulation without real world labels. In *2019 International Conference on Robotics and Automation (ICRA)*, pages 4818–4824. IEEE, 2019.
- [7] Mariusz Bojarski, Davide Del Testa, Daniel Dworakowski, Bernhard Firner, Beat Flepp, Praseon Goyal, Lawrence D Jackel, Mathew Monfort, Urs Muller, Jiakai Zhang, et al. End to end learning for self-driving cars. *arXiv preprint arXiv:1604.07316*, 2016.
- [8] Alexander Domahidi, Aldo U Zraggen, Melanie N Zeilinger, Manfred Morari, and Colin N Jones. Efficient interior point methods for multistage problems arising in receding horizon control. In *51st IEEE Conference on Decision and Control*, pages 668–674. IEEE, 2012.
- [9] Samira S Farahani, Vasumathi Raman, and Richard M Murray. Robust model predictive control for signal temporal logic synthesis. In *Conference on Analysis and Design of Hybrid Systems (ADHS)*, pages 323–328. IFAC, 2015.
- [10] Anders Forsgren, Philip E Gill, and Margaret H Wright. Interior methods for nonlinear optimization. *SIAM Review*, 44(4):525–597, 2002.
- [11] Xiaojun Geng and Yugeng Xi. Suboptimality analysis of receding horizon predictive control with terminal constraints. *IFAC Proceedings Volumes*, 32(2):2984–2988, 1999.
- [12] Philip E Gill, Walter Murray, and Michael A Saunders. Snopt: An SQP algorithm for large-scale constrained optimization. *SIAM Review*, 47(1):99–131, 2005.
- [13] Ignacio E Grossmann, VT Voudouris, and Omar Ghattas. Mixed-integer linear programming reformulations for some nonlinear discrete design optimization problems. *Technical Report, Carnegie Mellon University*, 1991.
- [14] Lars Grune and Anders Rantzer. On the infinite horizon performance of receding horizon controllers. *IEEE Transactions on Automatic Control*, 53(9):2100–2111, 2008.
- [15] LLC Gurobi Optimization. Gurobi optimizer reference manual, 2019.
- [16] Mohammadhosein Hasanbeig, Yiannis Kantaros, Alessandro Abate, Daniel Kroening, George J Pappas, and Insup Lee. Reinforcement learning for temporal logic control synthesis with probabilistic satisfaction guarantees. *arXiv preprint arXiv:1909.05304*, 2019.
- [17] Xiaowei Huang, Marta Kwiatkowska, Sen Wang, and Min Wu. Safety verification of deep neural networks. In *International Conference on Computer Aided Verification*, pages 3–29. Springer, 2017.
- [18] Martin Keller, Frank Hoffmann, Carsten Hass, Torsten Bertram, and Alois Seewald. Planning of optimal collision avoidance trajectories with timed elastic bands. *IFAC Proceedings Volumes*, 47(3):9822–9827, 2014.
- [19] Philip Koopman and Michael Wagner. Challenges in autonomous vehicle testing and validation. *SAE International Journal of Transportation Safety*, 4(1):15–24, 2016.
- [20] Ailsa H Land and Alison G Doig. An automatic method for solving discrete programming problems. In *50 Years of Integer Programming 1958-2008*, pages 105–132. Springer, 2010.
- [21] Nancy Leveson. Are you sure your software will not kill anyone? *Communications of the ACM*, 63(2):25–28, 2020.
- [22] Matt Luckcuck, Marie Farrell, Louise A Dennis, Clare Dixon, and Michael Fisher. Formal specification and verification of autonomous robotic systems: A survey. *ACM Computing Surveys (CSUR)*, 52(5):1–41, 2019.
- [23] Arnold Neumaier. Complete search in continuous global optimization and constraint satisfaction. *Acta Numerica*, 13:271–369, 2004.
- [24] Jorge Nocedal and Stephen Wright. *Numerical optimization*. Springer Science & Business Media, 2006.
- [25] Jérémy Omer and Jean-Loup Farges. Hybridization of nonlinear and mixed-integer linear programming for aircraft separation with trajectory recovery. *IEEE Transactions on Intelligent Transportation Systems*, 14(3):1218–1230, 2013.
- [26] Dorsa Sadigh and Ashish Kapoor. Safe control under uncertainty with probabilistic signal temporal logic. In *Robotics: Science and Systems*, 2016.
- [27] Wilko Schwarting, Javier Alonso-Mora, Liam Paull, Serdac Karaman, and Daniela Rus. Safe nonlinear trajectory generation for parallel autonomy with a dynamic vehicle model. *IEEE Transactions on Intelligent Transportation Systems*, 19(99), 2017.
- [28] Sanjit A Seshia, Dorsa Sadigh, and S Shankar Sastry. Towards verified artificial intelligence. *arXiv preprint arXiv:1606.08514*, 2016.
- [29] Martin Treiber, Ansgar Hennecke, and Dirk Helbing. Congested traffic states in empirical observations and microscopic simulations. *Physical Review E*, 62(2):1805, 2000.
- [30] Robert J Vanderbei and David F Shanno. An interior-

point algorithm for nonconvex nonlinear programming. *Computational Optimization and Applications*, 13(1-3):231–252, 1999.

- [31] Andreas Wächter and Lorenz T Biegler. On the implementation of an interior-point filter line-search algorithm for large-scale nonlinear programming. *Mathematical Programming*, 106(1):25–57, 2006.
- [32] H Paul Williams. *Model building in mathematical programming*. John Wiley & Sons, 2013.
- [33] Changxi You, Jianbo Lu, Dimitar Filev, and Panagiotis Tsiotras. Advanced planning for autonomous vehicles using reinforcement learning and deep inverse reinforcement learning. *Robotics and Autonomous Systems*, 114:1–18, 2019.

APPENDIX

A. Optimization parameters

The parameters used in the solving of Problem 2 and 3 in the context of Sec. V are defined in Table 1.

Parameter	Stage	Value	Parameter	Stage	Value
L	NLP	4.8	a_{\min}^x	MILP	-3
δ_{\max}	NLP	0.45	a_{\max}^x	MILP	3
a_{\min}	NLP	-3	a_{\min}^y	MILP	-0.5
a_{\max}	NLP	3	a_{\max}^y	MILP	0.5
\dot{a}_{\max}	NLP	0.5	Δa_{\max}^x	MILP	0.5
$\dot{\delta}_{\max}$	NLP	0.18	Δa_{\max}^y	MILP	0.1
\dot{a}_{\max}	NLP	0.5	v_{\min}^x	MILP	0
v_{\min}	NLP	0	v_{\max}^x	MILP	3
v_{\max}	NLP	10	v_{\min}^y	MILP	-1
ω_x	NLP	0.1	v_{\max}^y	MILP	1
ω_v	NLP	2.5	Ω_x	MILP	0.9
ω_y	NLP	0.05	Ω_v	MILP	0.5
ω_a	NLP	1.0	Ω_y	MILP	0.05
ω_δ	NLP	2.0	Ω_a	MILP	0.4
ρ	MILP	1.5	M	MILP	10^4
d	MILP	0.9			

TABLE A1: Parameters used in the MILP and NLP optimization stages

B. Generation of scenario examples

For the randomly generated scenarios presented in Sec. V, we assume the ego vehicle has length $4.8m$ and width $1.9m$. The examples used in this work were procedurally generated by uniformly sampling the parameters of the scenarios, following the ranges defined in Tables B1, B2, B3, B4 and B5.

Parameter	Min	Max
Number of lanes	2	2
Lane width (m)	3.5	4.3
Ego initial x (m)	0	0
initial y (m)	$b_l(x) + 0.55 * 1.9$	$b_r(x) - 0.55 * 1.9$
initial v (ms^{-1})	0	9.5
initial ϕ (rad)	$-\pi/12$	$+\pi/12$

TABLE B1: Common parameters

Parameter	Min	Max
Number of static vehicles	2	6
Static vehicle x (m)	0	80
y (m)	$b_l(x)$	$b_r(x)$
width (m)	1.7	2.5
length (m)	4.0	8.0

TABLE B2: Parameters of scenario SO

Parameter	Min	Max
Number of static vehicles	2	6
Static vehicle x (m)	0	80
y (m)	$b_l(x)$	0
width (m)	1.7	2.5
length (m)	4.0	8.0
Oncoming vehicle initial x (m)	20	80
initial y (m)	$b_r(x)/2$	$b_r(x)/2$
initial v (ms^{-1})	1.0	8.5
width (m)	1.7	2.5
length (m)	4.0	8.0

TABLE B3: Parameters of scenario SO+OV

Parameter	Min	Max
Dynamic vehicle initial x (m)	20	80
initial y (m)	$b_l(x)/2$	$b_l(x)/2$
initial v (ms^{-1})	0.5	3.5
width (m)	1.7	2.5
length (m)	4.0	8.0

TABLE B4: Parameters of scenario DO

Parameter	Min	Max
Oncoming vehicle initial x (m)	20	80
initial y (m)	$b_r(x)/2$	$b_r(x)/2$
initial v (ms^{-1})	1.0	8.5
width (m)	1.7	2.5
length (m)	4.0	8.0
Dynamic vehicle initial x (m)	20	80
initial y (m)	$b_l(x)/2$	$b_l(x)/2$
initial v (ms^{-1})	0.5	3.5
width (m)	1.7	2.5
length (m)	4.0	8.0

TABLE B5: Parameters of scenario DO+OV